We Want Our Photons Back: Simple Nanostructures for White Organic Light-Emitting Diode Outcoupling

Yong Hyun Kim, Jonghee Lee, Won Mok Kim, Cornelius Fuchs, Simone Hofmann, Hong-Wei Chang, Malte C. Gather, Lars Müller-Meskamp, and Karl Leo**

Conventional planar organic light-emitting diodes (OLEDs) suffer from poor light extraction due to the total internal reflection at the waveguided interfaces. Therefore, the development of efficient light extraction structures is of great necessity and significance to realize practical applications in large area and cost-effective light sources. In this paper, a high-performance internal light outcoupling system for white OLEDs with spontaneously formed metal oxide nanostructures is developed. The fabrication process of the outcoupling system is simple and can be scaled to large area manufacturing. The enhancement of external quantum efficiency in white OLEDs comprising the outcoupling system reaches a factor of 1.7, and it is further increased to 2.9 when a hemispherical lens is employed. Together with the improvement of light extraction, excellent color stability over broad viewing angles is achieved.

1. Introduction

White organic light-emitting diodes (OLEDs) have attracted much attention in recent years due to their potential as low-cost and high efficiency light sources.[1–5] With the use of phosphorescent emitter materials, the internal quantum efficiency (IQE) of OLEDs has reached nearly 100%.[6,7] However, a large number of photons are still trapped inside the device, mainly due to a large refractive index mismatch at the interfaces and surface plasmon coupling at the metal electrode.[8,9] Classical ray optics shows that the ratio of outcoupled photons is limited to only about 20% in conventional planar bottom-emitting OLEDs.[10–12] The low light outcoupling efficiency severely limits the potential of OLEDs and calls for an efficient light extraction structure.

Much progress has been achieved for light trapped in the substrate, where simple microscopic structures such as lens arrays can significantly improve outcoupling.[13–15] In contrast, outcoupling of the waveguide modes trapped in the organics/electrode thin films is much more challenging for two reasons: First, one has to integrate a scattering structure in the active layers which potentially hampers their electrical functions. Second, structures on the order of the wavelength in these layers, i.e. on the nanoscale, are needed. These are in particular challenging for white OLED for applications, where these nanostructures must interact with a broad spectrum, provide a color-stable angular spectrum, and remain compatible with low-cost large area fabrication. Despite significant efforts using approaches such as low index grids,[16] scattering layers,[17–21] textured substrates,[22] corrugated substrates,[23,24] photonic crystals,[25] and microlenses,[13–15,26,27] most techniques still involve complicated and expensive fabrication processes, and are limited to small area or monochromic emission, which is not acceptable for practical applications. The alternative approach of using high refractive index substrates ($n \geq 1.8$)[4,28] is not suitable for low-cost production due to their high-cost and undesirably large total internal reflection at the air/glass substrate interface. The approach of reducing optical microcavity effects and suppressing waveguide modes by using a low refractive index conductive polymer or an oxide/metal/oxide electrode concept[29,30] is attractive, but significantly limits the material choices and must be combined with other methods. In summary, a real breakthrough in form of low-cost, wavelength- and angle independent, and highly efficient nanostructures for outcoupling in white OLED has not been achieved.

Here, we report a novel concept to strongly improve the performance of white OLEDs based on a combination of readily fabricated internal light extraction system composed of a metal oxide nanostructure and a highly conductive low refractive index polymer electrode. The use of the conductive polymer electrode

Dr. Y. H. Kim, Dr. L. Müller-Meskamp, Prof. K. Leo
Dresdner Innovationszentrum für Energieeffizienz
Institut für Angewandte Photophysik
Technische Universität Dresden
01062 Dresden und Fraunhofer
COMEDD, 01109, Dresden, Germany
E-mail: yong.hyun.kim@iapp.de; leo@iapp.de
Dr. Y. H. Kim, Dr. J. Lee, C. Fuchs, Dr. S. Hofmann,
Dr. H.-W. Chang, Prof. M. C. Gather,
Dr. L. Müller-Meskamp, Prof. K. Leo
Institut für Angewandte Photophysik
Technische Universität Dresden
01062, Dresden, Germany
Dr. Y. H. Kim
Department of Imaging System Engineering
Pukyong National University
Busan, Republic of Korea
Dr. J. Lee
OLED Research Center
Electronics and Telecommunications Research Institute (ETRI)
Daejeon, 305–700, Republic of Korea
Dr. W. M. Kim
Electronic Materials Research Center
Korea Institute of Science and Technology
39–1, Hawolgok-dong, Sungbuk-gu, Seoul, 136–791, Republic of Korea

DOI: 10.1002/adfm.201303401

enables a fabrication of low-cost and flexible devices by replacing the conventional indium tin oxide (ITO) electrode which is expensive and brittle. The combined beneficial effects of refractive index matching, corrugated structure, and light scattering allow a significant enhancement of the external quantum efficiency (EQE) by a factor of 1.7, even at a high brightness of 10 000 cd m^{-2}. To the best of our knowledge, this enhancement is the largest reported for white OLEDs with internal scattering structures. The enhancement factor can be further increased to 2.9 when a hemispherical lens is used to extract all light from the glass substrate. Furthermore, the color stability over viewing angle is also significantly improved by the light outcoupling system. We believe that this novel light outcoupling system is a key step towards low-cost and high efficiency white OLEDs.

2. Results and Discussion

The facile manufacturing process of our light extraction layers, consisting of metal oxide nanostructures, is shown in **Figure 1**a. 300 nm thick tin (Sn) metal films are deposited on the glass substrate by standard magnetron sputtering. By annealing the films in vacuum, the metal films melt and agglomerate on the glass surface driven by thermal energy, thus forming a nanocluster structure as shown in scanning electron microscope (SEM) images (Figure 1c). The films are subsequently annealed at 500 °C in air to achieve complete oxidation of the films. The resulting films show randomly distributed metal oxide nanoclusters with particle size from a few hundred nanometers to a few micrometers. The integration of such an internal scattering structure into OLEDs is challenging since the large surface roughness of the nanostructures frequently leads to substantial leakage currents. To overcome this issue, a micrometer-thick transparent planarization polymer with a refractive index of around 1.52~1.55 across the visible wavelength range is spun onto the metal oxide nanoclusters. We refer to this metal oxide-based light extraction system as MOLES in the following.

The total (specular + diffuse) and diffuse transmittance of the scattering system is shown in **Figure 2**a. At a wavelength of 550 nm the oxidized Sn film shows a total and

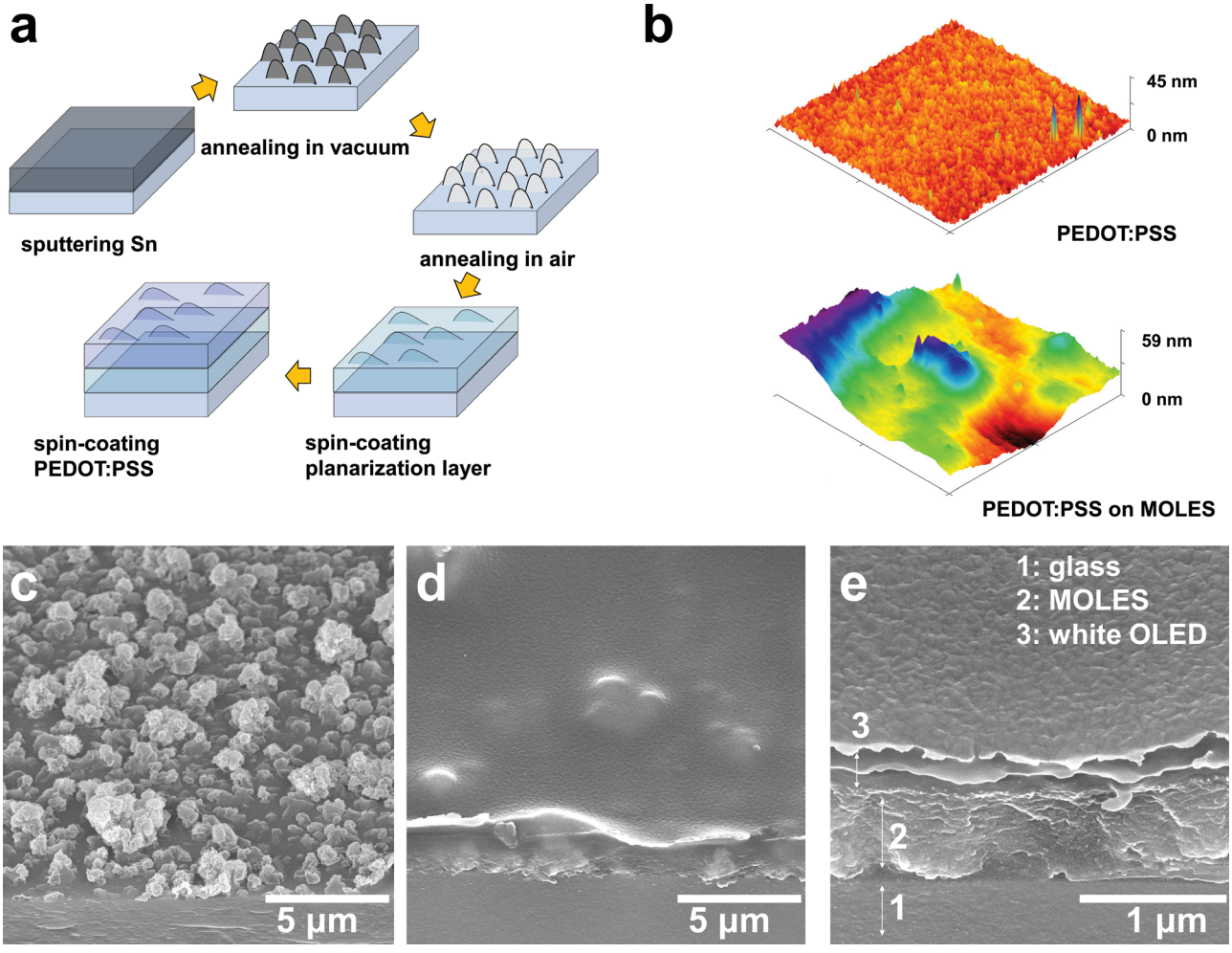

Figure 1. (a) Schematic process flow for spontaneously formed metal oxide-based light extraction systems (MOLES). (b) AFM images of PEDOT:PSS polymer electrodes on planar glass and on MOLES (6 × 6 μm^2). Tilted SEM images of (c) metal oxide scattering films without planarization layers and (d,e) white OLEDs on MOLES.

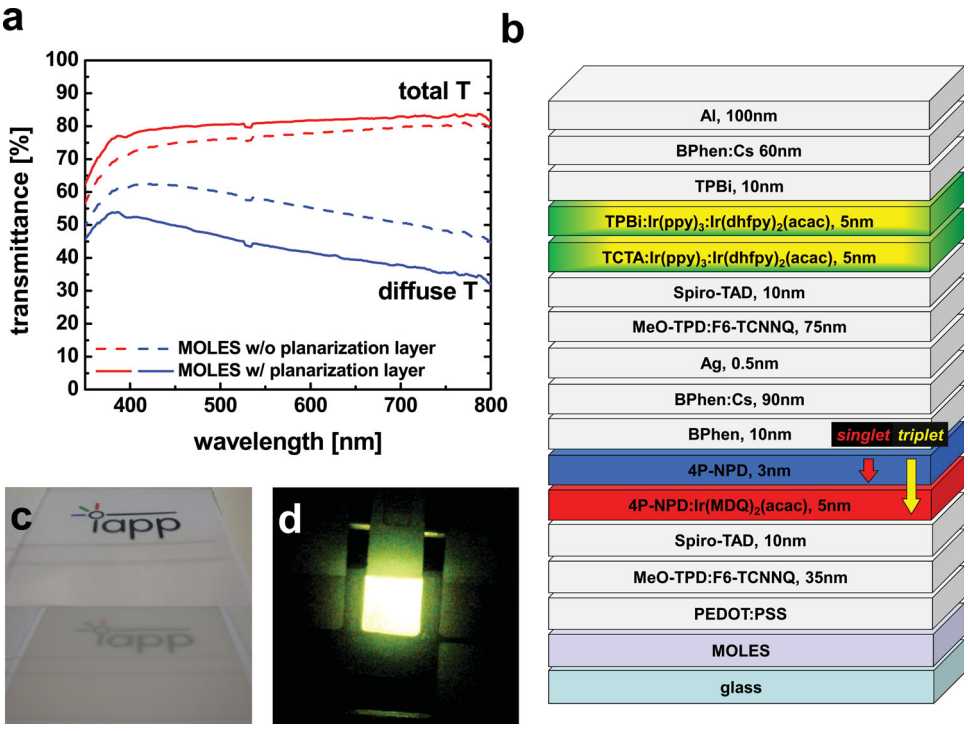

Figure 2. (a) Transmittances of the scattering film with and without planarization layer. (b) Device structures of white OLEDs with MOLES. (c) Photographs of (top) bare glass and (bottom) scattering film without planarization layers, placed on the institute logo. (d) Photograph of a white OLED with embedded MOLES.

diffuse transmittance of 77.0 and 57.6%, respectively. The high total (i.e., low absorption) and high diffuse (i.e., large scattering effects) transmittance of these light outcoupling films should greatly increase the light outcoupling from the OLEDs while introducing only small optical absorption losses. After coating the planarization layer, the total transmittance slightly increases, but the diffuse transmittance decreases by more than 10% because of a reduced refractive index difference between the surrounding media and the scattering nanoparticles. Nevertheless, the diffuse transmittance is large enough to achieve efficient light scattering. The uniformity of the scattering films turns out to be excellent since the initial metal films are homogeneously sputtered, thus illustrating the potential for easy scaling of the process in practical production settings (Figure 2c).

For the transparent bottom electrode on top of the MOLES, we use highly conductive poly(3,4-ethylenedioxythiophene):poly (styrenesulfonate) (PEDOT:PSS). This minimizes the refractive index mismatch as the refractive index of PEDOT:PSS (n ~ 1.5 at the visible wavelength range) is similar to that of the planarization polymer. Therefore, the internal reflection between the electrode and the MOLES is significantly reduced compared to the use of ITO (n ~ 2.0). Moreover, waveguide modes which trap photons in between the glass substrate (n ~ 1.5) and the electrode can be notably suppressed by using the low refractive index PEDOT:PSS electrode. In addition, the weak microcavity effect in PEDOT:PSS-based OLEDs can reduce waveguide modes as described by Cai et al.[31] Our previous studies showed comparable or even better performance of organic opto-electronic devices based on highly conductive PEDOT:PSS electrodes in comparison with ITO electrodes for applications in organic solar cells as well as OLEDs.[29,32–34]

Figure 1b shows atomic force microscopy (AFM) images of MOLES with the electrode coating on top. It is found that the corresponding root mean square (RMS) roughness of the electrode on top of our MOLES is around 6 nm, which is sufficiently smooth to avoid electrical short in our devices. It is notable that these MOLES have spontaneously corrugated and grooved surfaces despite of the planarization layer. These structures are caused by the embedded metal oxide nanoclusters as shown in AFM and SEM images (Figure 1) and will contribute to interface scattering. In addition, the metal oxide nanoclusters (n ~ 2.0)[35] offer a high optical contrast with respect to the underlying glass (n ~ 1.5) and the planarization layer deposited on top (n = 1.52~1.55) and thus will act as strongly scattering objects. The smooth corrugated surface as well as the light scattering effect by the high refractive index nanoparticles is one of the key factors to improve the performance of white OLEDs as discussed in the following.

As next step, we fabricate white OLEDs on top of the combination of MOLES and PEDOT:PSS electrodes. The white OLEDs stack consisting of a green/yellow unit and an efficient triplet harvesting blue/red unit in a tandem structure is optimized for high performance.[36] Three different systems are used in this experiment: The Device_ITO is a reference device with an ITO electrode without MOLES. The Device_PEDOT is a reference with a PEDOT:PSS electrode without MOLES. The Device_MOLES is based on a PEDOT:PSS electrode on top of the MOLES.

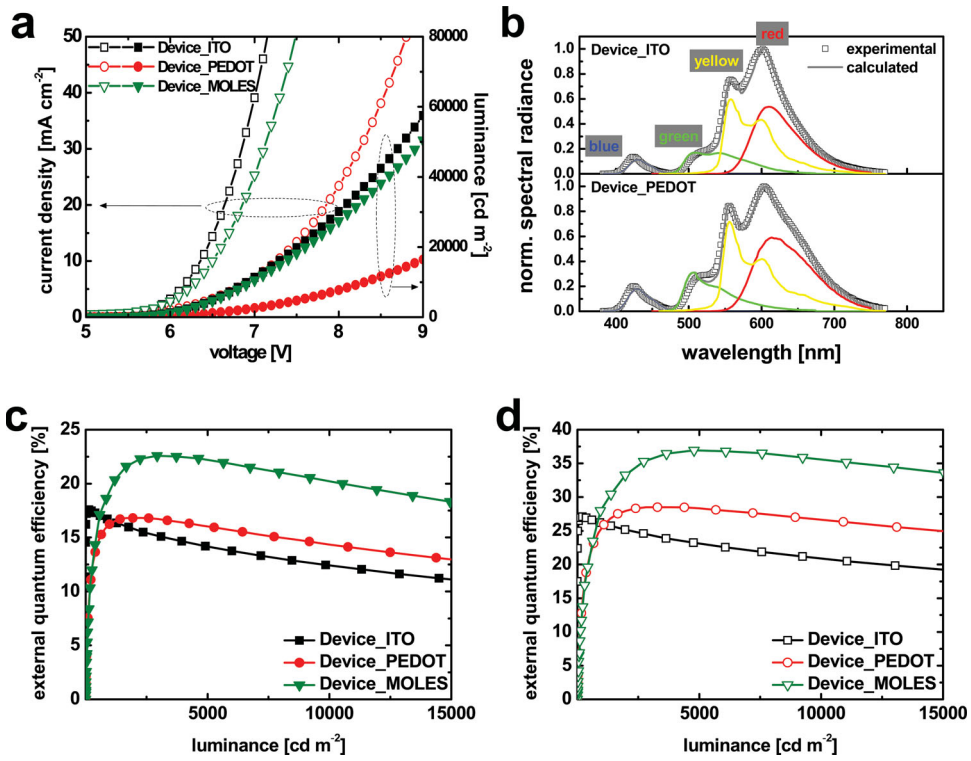

Figure 3. (a) Current density and luminance spectra as a function of driving voltage. (b) Experimental and calculated electroluminescence spectrum. The external quantum efficiency as a function of luminance for white OLEDs (c) without and (d) with a hemispherical lens.

The current density-voltage-luminance (*J-V-L*) characteristics of all three types of devices are shown in **Figure 3**a. When comparing the two reference devices based on ITO and PEDOT:PSS electrodes, the influence of the bottom electrodes on the OLEDs performance is clearly visible. The Device_PEDOT shows higher operating voltages compared to the reference Device_ITO due to the relatively lower conductivity of PEDOT:PSS which leads to reduced luminance, in particular at high voltages. Although this means that the luminous efficacy of the Device_PEDOT (13.1 lm W^{-1}) is slightly lower than that of the Device_ITO (14.5 lm W^{-1}), the EQE of the Device_PEDOT (14.3%) is actually higher than that of the Device_ITO (12.3%), even at a brightness of 10 000 cd m^{-2}. This enhancement is mainly caused by the fact that the PEDOT electrode suppresses waveguide modes due to the weak microcavity effect and the relatively well-matched refractive index between glass, PEDOT:PSS, and the organic layers as discussed earlier. At low luminances, the Device_PEDOT and the Device_MOLES show lower efficiencies compared to the Device_ITO because of leakage currents at the edge of PEDOT:PSS electrodes which are laterally patterned by laser ablation. Figure 3b shows the experimental and simulated electroluminescence spectrum for the Device_ITO and the Device_PEDOT. Four emitters (red, blue, green, and yellow) are fitted by the measured emission spectrum.[37] The calculated spectrally integrated outcoupling efficiencies of the Device_ITO and the Device_PEDOT are 21.7 and 23.1%, respectively.

Compared to the two reference devices, the Device_MOLES shows greatly improved EQE as shown in Figure 3c and summarized in **Table 1**. The EQE of the Device_MOLES reaches over 20.3% at a brightness of 10 000 cd m^{-2}, an improvement by a factor of 1.7 with respect to the reference Device_ITO. To our knowledge, this enhancement factor is one of the highest values reported for white OLEDs without any additional external outcoupling structures at high brightness conditions. To investigate this in more detail and to extract photons trapped

Table 1. Parameters of white OLEDs at 10 000 cd m^{-2} based on the reference and different types of MOLES. The enhancement values are calculated from the reference Device_ITO (marked "-") without a hemispherical lens.

	w/o hemispherical lens			w/ hemispherical lens		
@10 000 cd m^{-2}	lm W^{-1}	EQE	EQE enhancement	lm W^{-1}	EQE	EQE enhancement
Device_ITO	14.5	12.3	–	25.4	20.8	1.8
Device_PEDOT	13.1	14.3	1.2	26.1	26.6	2.2
Device_MOLES	22.7	20.3	1.7	41.6	35.6	2.9

within the glass substrate, an index-matched hemispherical lens is applied to the glass substrate and the efficiency of the devices is measured again, using an integrating sphere and a constant current level. As summarized in Table 1, the Device_MOLES shows significantly increased EQE from 20.3 to 35.6% (EQE increase of 15.3%) by the hemispherical lens, while the EQE of the reference Device_ITO increases from 12.3 to 20.8% when attaching the hemispherical lens (EQE increase of 8.5%). We attribute this to very efficient scattering of waveguide modes into the glass substrate by the MOLES which means that for the Device_MOLES much more light is confined in the glass substrate. Overall, the Device_MOLES shows a dramatic improvement of EQE, by a factor of 2.9, compared to the reference Device_ITO without the lens at the high brightness of 10 000 cd m^{-2} (Figure 3d).

It is interesting to note that the Device_MOLES shows a greatly reduced operating voltage which is far closer to that of the Device_ITO. This voltage reduction is attributed to the corrugated surface of our system as shown in AFM and SEM images. It is reported that corrugated substrates improve the current density of devices caused by a partially reduced organic layer thickness, i.e., enhances electric fields resulting from non-uniformity of the organic layer thicknesses.[23,38,39] The spontaneously formed corrugated surface structure of MOLES results in beneficial effects of better charge injection and reduction of the operating voltage. Therefore, the efficiency enhancement of the devices based on MOLES is attributed to the combined effects of the efficient light outcoupling by the internal light scattering system and the low operating voltage by spontaneously formed corrugated structures. The greatly enhanced luminance of the Device_MOLES compared to the Device_PEDOT indicates the efficient extraction of the waveguide modes (by the light scattering) apart from the improvement of electrical performance (by the corrugated surface). Furthermore, we highlight that the highly improved outcoupling efficiency in the high brightness region is very promising for practical lighting applications. As a further advantage, the total/diffuse transmittance and surface roughness of MOLES can be tuned by controlling the thickness, material, and composition ratio of alloy films as well as the surface energy of substrates which determines the magnitude of agglomeration of metal films (see Supporting Information), showing room for further improvement.

Besides the enhancement of light outcoupling efficiency, the color stability of the white OLEDs is also markedly improved by MOLES. **Figure 4**b shows the angular emission of the Device_MOLES. The emission dependence of the Device_MOLES on viewing angles is very small compared to the Device_ITO (Figure 4a), showing high quality white light. Figure 4c presents the change of the Commission Internationale del'Eclairage (CIE) color coordinates of the different devices with respect to the viewing angle. The Device_MOLES exhibits an extremely stable color point as a function of the viewing angle, indicating that MOLES drastically suppresses the color shift of the device due to re-distribution of photons by scattering.[19,20] We quantitatively describe the characteristics of color shift of the devices over viewing angles as described by Shama et al.[40] The quantitative color shift is calculated as the path integral in CIE-$L^*a^*b^*$ space weighted with the function of distance from the origin at angle = 0. The ratios of the calculated quantitative color shift

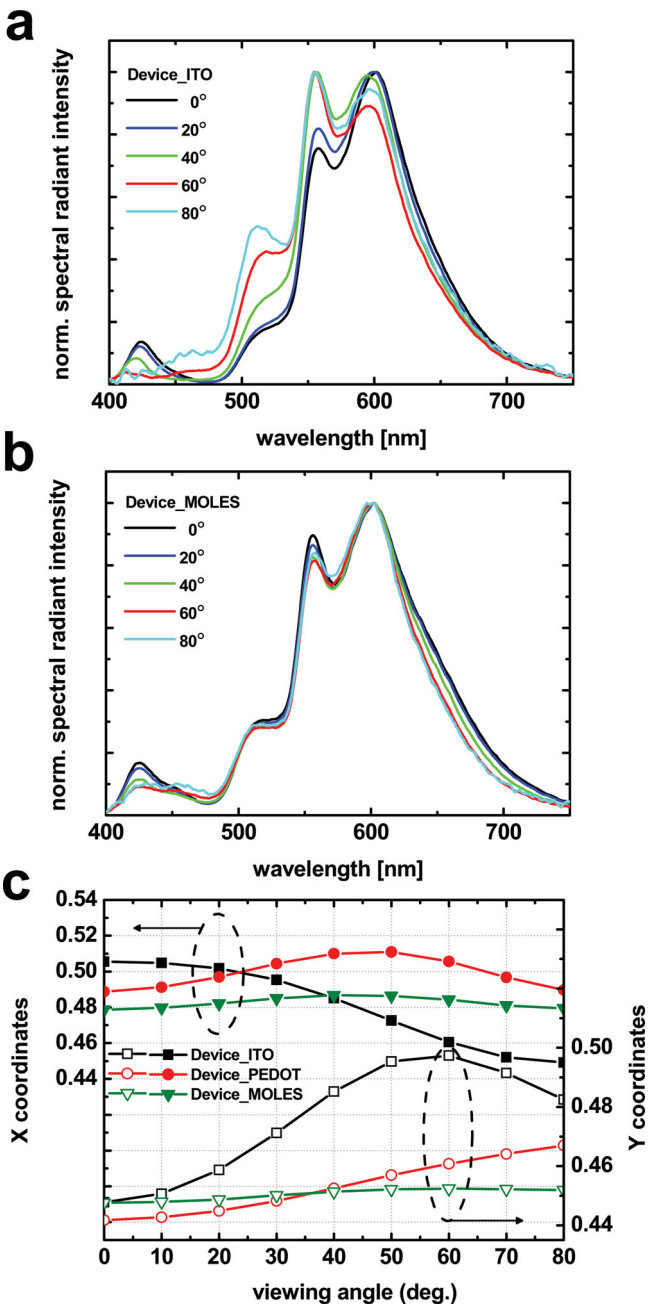

Figure 4. Normalized spectral emission intensity for (a) the Device_ITO and (b) the Device_MOLES for different viewing angle. (c) Shift in CIE coordinates over the viewing angle for the white OLEDs. Note the extremely small shift of the MOLES device.

taking all angles up to 60° into account for the Device_ITO and the Device_PEDOT to the Device_MOLES are 8.3 and 1.6 respectively, showing a remarkable enhancement of the color stability for the Device_MOLES. Stabilizing the color balance of white OLEDs is a very challenging task, due to the wide emission spectrum, but generally considered to be of great importance for practical applications. Thus, we believe that the excellent color stability achieved by scattering with MOLES is a step ahead for OLED development and that such a scattering

layer would significantly improve commercial, white OLED products.

3. Conclusions

We have developed a highly efficient internal light extraction and color stabilizing system by using a simple and easy manufacturing process. The metal oxide embedded nanostructures (MOLES) combined with a conductive polymer electrode show a superior refractive index matching from the organic layers to the substrate, form a corrugated surface, and provide excellent light scattering. This results in a 2.9-fold enhanced EQE for white OLEDs, even at a high luminance of 10 000 cd m^{-2} and leads to excellent color stability over a broad range of viewing angles. The enhanced performance is wavelength- and angle independent. Furthermore, an improvement in the lifetime of white OLEDs is expected as a direct result of the enhanced luminous efficacy. In addition to high performance, a significant reduction in the cost of device can be achieved by the use of the alternative conductive polymer electrode, which replaces the conventional ITO electrode. Although the high-temperature processing limits substrate availability, we expect MOLES to be a superior light extraction system in practical lighting applications because of its clear advantages. It should be highlighted that our approach is a very simple and easy method compared to other techniques, allowing low-cost production, reliable and high throughput, lithography-free and low-energy processing. The performance can be further improved by optimizing the size and distribution of metal oxide nanostructures, which are controlled by thickness, material, and composition of metal films. We believe that this simple, inexpensive, reliable, and highly reproducible system is a key technology and will greatly contribute the development of efficient, color-stable white OLEDs for lighting applications.

4. Experimental Section

Preparation and Characterization of the Metal Oxide-Based Light Extraction System (MOLES): 300 nm thick Sn films were deposited on glass at room temperature by radio frequency magnetron sputtering system. The prepared Sn films were annealed under vacuum (10^{-3} mbar) at 300 °C for 30 min, and subsequently annealed in air at 500 °C for 1 h. A propylene glycol-monomethyl-ether acetate-based photo-resist (Everlight Chemical Industrial Corporation), used as planarization polymer, was spun onto the fabricated metal oxide films. Afterwards, the spin-coated films were annealed on a hot plate at 130 °C for 10 min. As a conductive electrode, PEDOT:PSS (Clevios PH1000, Heraeus) mixed with 6 vol.% ethylene glycol was spin-coated on the scattering systems. The coated samples were baked at 120 °C for 15 min, as described in detail previously.[33,34] The transmittance was examined by a spectrophotometer (Shimadzu MPC3100). AFM images of the scattering systems were recorded in tapping mode (AIST-NT Combiscope). SEM images were taken by a Zeiss Gemini DSM 982.

Fabrication and Characterization of the White OLEDs: The small molecule organic layers were thermally evaporated on MOLES in an ultra-high vacuum chamber (K. J. Lesker, UK) at a base pressure of around 10^{-8} mbar. The used organic materials are purified by high-vacuum gradient sublimation. For the removal of residual water in the PEDOT:PSS electrode, the devices were heated at 110 °C for 30 min in the vacuum chamber, immediately before the evaporation of organic layers. The layer sequence used for the white OLEDs is as follows (from bottom to top):[36] glass substrate/MOLES/PEDOT:PSS/35 nm (*N,N,N′,N′*-tetrakis(4-methoxyphenyl)-benzidine) (MeO-TPD): 2,2′-(perfluoronaphthalene-2,6-diylidene)dimalononitrile (F6-TCNNQ) (2 wt%)/10 nm 2,2′,7,7′-tetrakis-(*N,N′*-diphenylamino)-9,9′-spirobifluorene (Spiro-TAD)/5 nm *N,N′*-di-1-naphthalenyl-*N,N′*-diphenyl-[1,1′:4′,1″:4″,1‴-Quaterpheny]l-4,4‴-diamine (4P-NPD): Iridium(III)bis(2-methyldibenzo-[f,h]chinoxalin)(acetylacetonat) ($Ir(MDQ)_2(acac)$) (5 wt%)/3 nm 4P-NPD/10 nm 4,7-diphenyl-1,10-phenanthroline (BPhen)/90 nm BPhen: Cs (1:1)/0.5 nm Ag/75 nm MeO-TPD: F6-TCNNQ (2 wt.%)/10 nm Spiro-TAD/5 nm 4,4′,4″-tris(*N*-carbazolyl)-triphenylamine (TCTA): fac-tris(2-phenylpyridine) iridium(III) ($Ir(ppy)_3$): bis(2-(9,9-dihexylfluorenyl)-1-pyridine) (acetylacetonate) iridium(III) ($Ir(dhfpy)_2(acac)$) (91:8:1 wt%)/5 nm 2,2'2″-(1,3,5-benzenetriyl)-tris[1-phenyl-1H-benzimidazole] (TPBi): $Ir(ppy)_3$: $Ir(dhfpy)_2(acac)$ (91:8:1 wt%)/10 nm TPBi/60 nm BPhen: Cs (1:1)/100 nm Al. After device fabrication, all devices were encapsulated with glass lids. The efficiency of Device_ITO was not as high as that reported previously due to partial deviation of a layer thickness.[36] However, the results were repeatable and reference samples were proven to be reasonable in other series of experiments.

Current-voltage-luminance characteristics and electroluminescence spectra were taken using an automated measurement setup with a source measurement unit and a calibrated CAS140CT spectrometer (Instrument Systems GmbH). External quantum efficiency and luminous efficacy were calculated with the spatial emission of devices, measured by a spectrogoniometer. The emission characteristics of the devices were examined at angles from 0° to 90°. The integrated external quantum efficiency and luminous efficacy were determined by a spectrometer measurement in the integrating sphere setup. To extract light trapped in the glass mode, a hemispherical lens (a diameter of 1.6 cm) was mounted on the substrate with index-matching immersion oil (Zeiss, 518F n = 1.518).

Supporting Information

Supporting Information is available from the Wiley Online Library or from the author.

Acknowledgements

Y. H. Kim and J. Lee contributed equally to this work. The authors thank O. R. Hild and C. May at Fraunhofer COMEDD for supporting the DIZEeff, and J. Blochwitz-Nimoth for his fruitful comments. This work was funded by the European Union (EFRE), the Fraunhofer Gesellschaft, and the Free State of Saxony as part of the Dresdner Innovationszentrum Energieeffizienz. This work was supported partially by the Korea Institute of Science and Technology (KIST) internal project under contract 2E22832. J. Lee acknowledges the Alexander von Humboldt Foundation and the IT R&D program of MSIP/KEIT (Grant No. 10041416).

Received: October 2, 2013
Revised: November 8, 2013
Published online: December 11, 2013

[1] T.-H. Han, Y. Lee, M.-R. Choi, S.-H. Woo, S.-H. Bae, B. H. Hong, J.-H. Ahn, T.-W. Lee, *Nat. Photonics* **2012**, *6*, 105.
[2] S. J. Su, E. Gonmori, H. Sasabe, J. Kido, *Adv. Mater.* **2008**, *20*, 4189.
[3] M. C. Gather, A. Köhnen, K. Meerholz, *Adv. Mater.* **2011**, *23*, 233.
[4] S. Reineke, F. Lindner, G. Schwartz, N. Seidler, K. Walzer, B. Lüssem, K. Leo, *Nature* **2009**, *459*, 234.
[5] Y. Sun, N. C. Giebink, H. Kanno, B. Ma, M. E. Thompson, S. R. Forrest, *Nature* **2006**, *440*, 908.

[6] C. Adachi, M. A. Baldo, M. E. Thompson, S. R. Forrest, *J. Appl. Phys.* **2001**, *90*, 5048.
[7] M. Baldo, D. O'brien, Y. You, A. Shoustikov, S. Sibley, M. Thompson, S. R. Forrest, *Nature* **1998**, *395*, 151.
[8] M. Furno, R. Meerheim, S. Hofmann, B. Lüssem, K. Leo, *Phys. Rev. B* **2012**, *85*, 115205.
[9] R. Meerheim, M. Furno, S. Hofmann, B. Lüssem, K. Leo, *Appl. Phys. Lett.* **2010**, *97*, 253305.
[10] N. C. Greenham, R. H. Friend, D. D. C. Bradley, *Adv. Mater.* **2004**, *6*, 491.
[11] G. Gu, D. Garbuzov, P. Burrows, S. Venkatesh, S. R. Forrest, M. Thompson, *Opt. Lett.* **1997**, *22*, 396.
[12] L. H. Smith, J. A. Wasey, I. D. Samuel, W. L. Barnes, *Adv. Funct. Mater.* **2005**, *15*, 1839.
[13] S. Möller, S. R. Forrest, *J. Appl. Phys.* **2002**, *91*, 3324.
[14] Y. Sun, S. R. Forrest, *J. Appl. Phys.* **2006**, *100*, 073106.
[15] M. Thomschke, S. Reineke, B. Lüssem, K. Leo, *Nano Lett.* **2012**, *12*, 424.
[16] Y. Sun, S. R. Forrest, *Nat. Photonics* **2008**, *2*, 483.
[17] B. Riedel, Y. Shen, J. Hauss, M. Aichholz, X. Tang, U. Lemmer, M. Gerken, *Adv. Mater.* **2011**, *23*, 740.
[18] H.-W. Chang, J. Lee, S. Hofmann, Y. Hyun Kim, L. Muller-Meskamp, B. Lussem, C.-C. Wu, K. Leo, M. C. Gather, *J. Appl. Phys.* **2013**, *113*, 204502.
[19] K. Hong, H. K. Yu, I. Lee, K. Kim, S. Kim, J. L. Lee, *Adv. Mater.* **2010**, *22*, 4890.
[20] T. Nakamura, H. Fujii, N. Juni, N. Tsutsumi, *Optical Rev.* **2006**, *13*, 104.
[21] T. Yamasaki, K. Sumioka, T. Tsutsui, *Appl. Phys. Lett.* **2000**, *76*, 1243.
[22] B. Riedel, I. Kaiser, J. Hauss, U. Lemmer, M. Gerken, *Optics Express* **2010**, *18*, A631.
[23] W. H. Koo, S. M. Jeong, F. Araoka, K. Ishikawa, S. Nishimura, T. Toyooka, H. Takezoe, *Nat. Photonics* **2010**, *4*, 222.
[24] B. J. Matterson, J. M. Lupton, A. F. Safonov, M. G. Salt, W. L. Barnes, I. D. W. Samuel, *Adv. Mater.* **2001**, *13*, 123.
[25] Y. R. Do, Y. C. Kim, Y. W. Song, C. O. Cho, H. Jeon, Y. J. Lee, S. H. Kim, Y. H. Lee, *Adv. Mater.* **2003**, *15*, 1214.
[26] J. B. Kim, J. H. Lee, C. K. Moon, S. Y. Kim, J. J. Kim, *Adv. Mater.* **2013**, *25*, 3571.
[27] T.-W. Koh, H. Cho, C. Yun, S. Yoo, *Org. Electronics* **2012**, *13*, 3145.
[28] S. Mladenovski, K. Neyts, D. Pavicic, A. Werner, C. Rothe, *Optics Express* **2009**, *17*, 7562.
[29] K. Fehse, K. Walzer, K. Leo, W. Lövenich, A. Elschner, *Adv. Mater.* **2007**, *19*, 441.
[30] Z. Wang, M. Helander, J. Qiu, D. Puzzo, M. Greiner, Z. Hudson, S. Wang, Z. Liu, Z. Lu, *Nat. Photonics* **2011**, *5*, 753.
[31] M. Cai, Z. Ye, T. Xiao, R. Liu, Y. Chen, R. W. Mayer, R. Biswas, K. M. Ho, R. Shinar, J. Shinar, *Adv. Mater.* **2012**, *24*, 4337.
[32] Y. H. Kim, J. Lee, S. Hofmann, M. C. Gather, L. Müller-Meskamp, K. Leo, *Adv. Funct. Mater.* **2013**, *23*, 3763.
[33] Y. H. Kim, C. Sachse, M. Hermenau, K. Fehse, M. Riede, L. Müller-Meskamp, K. Leo, *Appl. Phys. Lett.* **2011**, *99*, 113305.
[34] Y. H. Kim, C. Sachse, M. L. Machala, C. May, L. Müller-Meskamp, K. Leo, *Adv. Funct. Mater.* **2011**, *21*, 1076.
[35] V. Dimitrov, S. Sakka, *J. Appl. Phys.* **1996**, *79*, 1736.
[36] T. C. Rosenow, M. Furno, S. Reineke, S. Olthof, B. Lussem, K. Leo, *J. Appl. Phys.* **2010**, *108*, 113113.
[37] M. Furno, T. C. Rosenow, M. C. Gather, B. Lussem, K. Leo, *Appl. Phys. Lett.* **2012**, *101*, 143304.
[38] M. Fujita, T. Ueno, K. Ishihara, T. Asano, S. Noda, H. Ohata, T. Tsuji, H. Nakada, N. Shimoji, *Appl. Phys. Lett.* **2004**, *85*, 5769.
[39] S. M. Jeong, F. Araoka, Y. Machida, Y. Takanishi, K. Ishikawa, H. Takezoe, S. Nishimura, G. Suzaki, *Jap. J. Appl. Phys.* **2008**, *47*, 4566.
[40] G. Sharma, W. Wu, E. N. Dalal, *Color Res. Appl.* **2005**, *30*, 21.